Van Meer, G., Gahmberg, C. G., Op den Kamp, J. A. F., & van Deenen, L. L. M. (1981) *FEBS Lett. 135*, 53–55.

Venien, C., & Le Grimellec, C. (1988) *Biochim. Biophys. Acta 942*, 159–168.

Verklcij, A. J., Zwaal, R. F. A., Roelofsen, B., Comfurius, P., Kastclijn, D., & van Deenen, L. L. M. (1973) *Biochim. Biophys. Acta 323*, 178–193.

Wang, C. T., Shia, Y. I., Chen, J. C., Tsai, W. J., & Yang, C. C. (1986) *Biochim. Biophys. Acta 856*, 244–258.

Wicland, F. T., Gleason, M. L., Serafini, T., & Rothman, J. A. (1987) *Cell 50*, 289–300.

Williamson, P., Algarin, L., Bateman, J., Choe, H.-R., & Schlegcl, R. A. (1985) *J. Cell. Physiol. 123*, 209–214.

Williamson, P., Antia, R., & Schlegel, R. A. (1987) *FEBS Lett. 219*, 316–320.

Xie, X., Stone, D. K., & Racker, E. (1984) *J. Biol. Chem. 259*, 11676–11678.

Zachowski, A., & Devaux, P. F. (1989) *Commun. Mol. Cell. Biophys. 6*, 63–90.

Zachowski, A., & Morot Gaudry-Talarmain, Y. (1990) *J. Neurochem. 55*, 1352–1356.

Zachowski, A., Favre, E., Cribier, S., Hervé, P., & Devaux, P. F. (1986) *Biochemistry 25*, 2585–2590.

Zachowski, A., Fellmann, P., Hervé, P., & Devaux, P. F. (1987a) *FEBS Lett. 223*, 315–320.

Zachowski, A., Herrmann, A., Paraf, A., & Devaux, P. F. (1987b) *Biochim. Biophys. Acta 897*, 197–200.

Zachowski, A., Henry, J. P., & Devaux, P. F. (1989) *Nature 340*, 75–76.

Zwaal, R. F. A. (1988) *News Physiol. Sci. 3*, 57–61.

Accelerated Publications

Experimentally Verifying Molecular Dynamics Simulations through Fluorescence Anisotropy Measurements[†]

P. H. Axelsen,[*,‡] E. Gratton,[§] and F. G. Prendergast[‡]

Department of Biochemistry and Molecular Biology, Mayo Clinic and Foundation, Rochester, Minnesota 55905, and Laboratory for Fluorescence Dynamics, Department of Physics, University of Illinois, Urbana, Illinois 61801

Received October 19, 1990; Revised Manuscript Received December 6, 1990

ABSTRACT: The fluorescence anisotropy decay of the single tryptophan residue in phospholipase A_2 was studicd by use of differential polarized phase fluorometry and computer simulations of protein dynamics. The results enable the verification of a simulated dynamic event by direct experimental measurement on the same time scale. When all hydrogen atoms are modeled explicitly, the simulations agree well with the experimental measurements. However, the measurements contradict simulations in which nonpolar hydrogens are incorporated into "extended" or "united" atoms. These simulations predict an anisotropy decay in excess of mcasured values and appear to seriously underestimate the electrostatic interactions occurring between water and aromatic side chains. The results support the general validity of studying protein dynamics with the molecular-mechanics approach and illustrate a potentially serious deficiency of simulations which do not explicitly model all hydrogen atoms.

The experimental verification of molecular dynamics simulations of specific protein motions has not been generally feasible due to the limited overlap between experimentally and computationally accessible time scales. Simulations can predict results which are impressively consistent with experimental data (e.g., free energy differences; Ghosh & McCammon, 1987; Bash et al., 1987), but differences in time scale between laboratory measurement and simulation mark such comparisons as precarious extrapolations. Recently, there have been significant advances in the theory and technology of frequency domain fluorometers which enable the direct measurement of subnanosecond photophysical events (Lakowicz et al., 1986; Gratton and vandeVen, submitted for publication). This, along with concomitant increases in available computational power, now make it feasible to extend simulations into an experimentally accessible time scale.

From a theoretical perspective, a particularly straightforward way to compare simulation and experiment is to simulate and measure the anisotropy decay of tryptophan (TRP) fluorescence in proteins. Detailed derivations of the decay function in computer simulations (Ichiye & Karplus, 1983) and in phase fluorometry (Weber, 1977) are available. In the case of ribonuclease T_1 (RNAse-T_1), we have shown that experimental data can falsify simulations of fluorescence anisotropy decay in which solvent is neglected (Axelsen et al., 1988). This comparison was of limited rigor, however, because it involved "limiting anisotropy" data, implicitly requiring an extrapolation from the experimental data into the time scale of the computer simulation. Furthermore, the single Trp at position 59 is largely buried within the protein matrix, effectively precluding extensive rotational activity.

By use of gigahertz-domain differential polarized phase fluorometry and computers capable of propagating molecular dynamics simulations into a comparable time scale, a much more rigorous comparison is possible. Phospholipase A_2 (PLA2) was chosen for study because the single Trp residue at position 3 is in an altogether different circumstance than Trp-59 in RNAse-T_1; in PLA2, Trp-3 is fully exposed to solvent and has no obvious steric basis for hindrance to side-chain rotation. Yet, NMR (Allegrini et al., 1985) and

quenching-resolved fluorescence emission anisotropy data (Eftink, 1983) both suggest that the rotational activity of the Trp-3 side chain is indeed hindered. We have measured the fluorescence anisotropy decay of Trp-3 to confirm the degree to which its rotation is hindered and have conducted molecular dynamics simulations in order to explain the physicochemical basis for this behavior.

A comparison of the simulation results and measured Trp fluorescence anisotropy decays shows that simulations using the polar hydrogen model ("polar-H", "extended-atom", or "united-atom" representation) cannot be reconciled with the experimental measurements, whereas the same measurements are in good agreement with simulations in which all hydrogens are modeled explicitly ("explicit-H" representation). The rotational activity of Trp-3 appears to be hindered by a specific interaction between the Trp-3 side chain and water. The polar-hydrogen model fails to demonstrate this interaction because of an inherently bland representation of aromatic ring electrostatics.

EXPERIMENTAL PROCEDURES

Crystal coordinates for porcine PLA2 were taken from entry 1P2P in the Brookhaven Protein Data Bank (Bernstein et al., 1977; Dijkstra et al., 1983). Trajectories were calculated with CHARMM (Brooks et al., 1983; distributed by Polygen Corp., Waltham, MA) by use of the stochastic boundary approach (Brooks et al., 1985) as applied previously (Axelsen et al., 1988; Axelsen & Prendergast, 1989). The explicit-H and polar-H residue topologies were each used in separate simulations. A 16-Å stochastic boundary was centered on atom C_β of Trp-3; the simulated system included 56 of 124 residues and 362 TIP3 water models. The calcium binding site was outside of the boundary and therefore deleted. The system was equilibrated for 20 ps at 300 K and run for 1000 ps. Anisotropy decays were derived from these trajectories in the manner reported previously (Ichiye & Karplus, 1983; Axelsen et al., 1988). Free energy calculations were performed by a combined thermodynamic perturbation and umbrella sampling technique (Haydock et al., 1990).

Experimental measurements were made on two samples of porcine PLA2 (from separate purifications) generously provided by Dr. Stuart Hendrikson of St. Olaf College (Northfield, MN) in 30 mM MOPS buffer with 1 mM $CaCl_2$ at pH 7.0 and 20 °C. The sample was illuminated at 295 nm with the output of a frequency-doubled mode-locked cavity-dumped rhodamine 6G dye laser (Coherent) pumped by a frequency-doubled Nd-YAG pulse laser (Coherent). Emitted light was collected by a 6.2-μm microchannel plate, and the output signal was analyzed for harmonic content. Light scattering data showed that the harmonic content is sufficient and the electronics are suitable for studies up to 10 GHz. Signal processing is preceded by frequency conversion to 40 Hz with super-heterodyne amplifiers. The software used to control the measurement reports modulation ratio (Λ), which is calculated by dividing the modulated signal intensities for perpendicular ($I_\perp$) and parallel ($I_\parallel$) orientations of the emission polarizer with respect to the excitation polarizer. The values represented in the plots constitute a complete (unselected) set and are used raw, i.e., not "fit" or processed further.

In general, the collection of some scattered light is unavoidable because the inherently low signal-to-noise ratio at high frequencies requires that we use a relatively wide-band emission filter. Consequently, phase measurements tend to be very distorted at high frequencies. The relative insensitivity of modulation measurements to scattered light at these high frequencies makes them far more suitable for comparison to
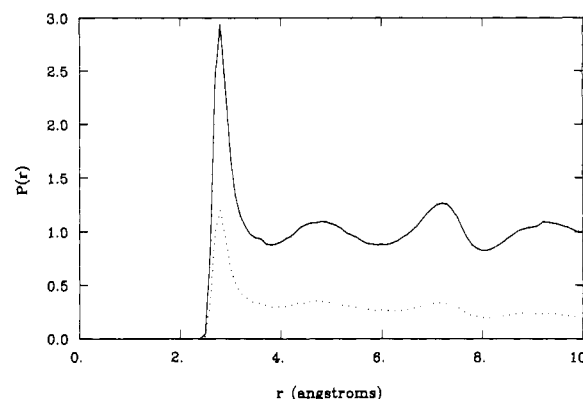

FIGURE 1: Oxygen–oxygen radial distribution functions for a 30-ps simulation of 216 water molecules in a periodic boundary at 300 K and a density of 0.03346 molecules/Å³ (solid line). Also shown is the corresponding distribution for water oxygens within the stochastic boundary of the explicit-H simulation (dashed line) showing that the primary, secondary, and tertiary peaks are positioned the same as in the periodic boundary. Peak height is, however, decreased because there is no water outside the boundary or in the space occupied by the protein.

the predictions made from molecular dynamics simulations. Hence, only modulation ratios are reported.

RESULTS

Simulations with explicit-H (1953 atoms) and polar-H (1453 atoms) models were initiated with the same (crystal) coordinates for the protein atoms and waters. Both were equilibrated with a 300 K "temperature bath" for 20 ps prior to the beginning of "data collection"; however, thermal stability of the simulation system was achieved within 0.5 ps in the polar-H simulation and within 10 ps in the explicit-H simulation. Each simulation was propagated for a total of 1000 ps beyond the equilibration period.

The density of water within a stochastic boundary is difficult to assess because of the protein atoms present. We have indirectly assessed the packing density by examining the radial distribution function of water oxygen atoms. Figure 1 shows the O–O radial distance distribution for a 30-ps simulation of 216 water molecules in a periodic boundary at 300 K and a density of 0.03346 molecules/Å³ (1 g/cm³). Also shown is the corresponding distribution for water oxygens within the stochastic boundary of the explicit-H simulation. We find that the primary, secondary, and tertiary peaks are positioned the same as in the periodic boundary. Peak height is, however, decreased because there is no water outside the boundary or in the space occupied by the protein.

The orientation of ^1L_a and ^1L_b transition dipole moments has been derived from glycyltryptophan crystals (Yamamoto & Tanaka, 1972), but we do not know the orientation of the emission moment, which can be ±25° of the absorption moment. For these reasons, we have assumed the position of maximum uncertainty on this matter and considered all possible orientations of μ_a with respect to the long axis of the side chain in 30° steps.

The anisotropy in the absence of motion (r_0) for Trp excited at 295 nm is taken to be 0.29 (Valeur & Weber, 1977), and μ_e is therefore oriented ±25° from μ_a. The time-dependent anisotropy decays were obtained by evaluating the second-order Legendre polynomial $\langle P_2 \rangle$ for half the length of the trajectory with each appropriate μ_a and μ_e pair (Axelsen et al., 1988). These decays are shown in Figure 2.

It is immediately clear that the simulations do not predict a unique anisotropy decay unless we are willing to assign specific orientations to μ_a and μ_e. Furthermore, many of the
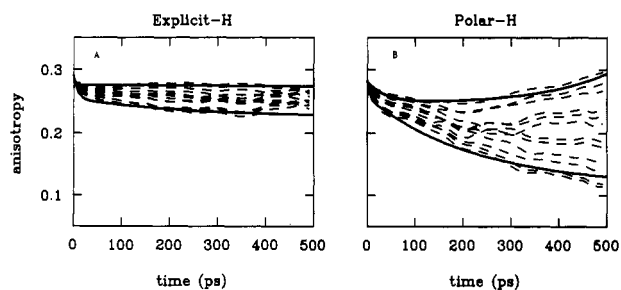
Explicit-H

Polar-H

FIGURE 2: Time-dependent anisotropy decay functions for (A) explicit-H and (B) polar-H trajectories. Each dashed line represents a decay function for μ_a oriented between 0° and 150° from the long axis of the side chain in 30-deg steps, and for μ_e oriented +25° and −25° relative to μ_a. The solid lines indicate least-square fits to the upper and lower curves with $r(t) = r_\infty + \alpha_1 \exp(-t/\phi_1) + \alpha_2 \exp(-t/\phi_2)$. The fitted parameter values are as follows:

parameter	explicit-H lower	explicit-H upper	polar-H lower	polar-H upper
r_∞	0.225	0.266	0.114	0.244
α_1	0.038	0.016	0.028	0.045
α_2	0.030	0.010	0.150	0.002
ϕ_1 (ps)	8.9	2.9	4.3	38.5
ϕ_2 (ps)	251.8	1959.0	233.0	−141.0

decay functions do not decrease monotonically, indicating either that the system has not been adequately equilibrated or that certain large-scale motions have not been sampled over sufficiently long times. This problem is markedly worse in the polar-H simulation (Figure 2B). We were unable to completely eliminate this problem by using only the last half of the trajectory for calculating the correlation function, implying that the latter half is no better "equilibrated" than the first half. This problem is discussed further below.

For the purpose of comparing experimental data to predictions of this nature, we fit double exponentials to the curves corresponding to minimum and maximum anisotropy decays, thereby defining an "envelope" of possible decay functions. In a realistic simulation, the experimental data should lie entirely within the bounds of such an envelope. This type of comparison requires that the function envelope be transformed from time domain anisotropy decay functions (as obtained from the simulation) into frequency domain functions and that terms for the overall rotation of the protein and the fluorescence intensity decay be added. These terms were incorporated

into expressions for the parallel and perpendicular light intensities as a function of time and analytically transformed into functions of frequency. The modulation ratio as a function of frequency, $\Lambda(\omega)$, may be calculated directly from the transformed intensity functions (see Appendix). The simulation results, processed in this way, may be compared directly to the raw experimental measurements without fitting of the experimental data.

Figure 3 shows how decay functions predicted by the simulations compare to raw experimental modulation ratio determinations made over a frequency range of 20–3000 MHz. It is clear that the experimental measurements lie within the envelope predicted by the explicit-H simulation (Figure 3A) but not within that predicted by the polar-H simulation (Figure 3B). These results suggest that the Trp side chain in the polar-H simulation exhibits rotations with unrealistically large amplitudes. The experimental measurements and the explicit-H simulation agree in both indicating that Trp rotations are comparatively hindered. Because the crystal structure does not suggest a clear reason why this rotational activity is hindered, we undertook to calculate the free energy barrier for rotation of Trp-3 on the surface of PLA2.

A technique which combines thermodynamic perturbation and umbrella sampling was used to explore the Helmholz free energy for rotation of the Trp side chain about its χ_1 (C_β–C_γ) bond (Haydock et al., 1990). This reaction coordinate was selected because a preliminary adiabatic potential surface map of χ_1 and χ_2 in vacuo suggested rather immediate and large steric barriers to simple rotation existed about χ_2. Therefore, an umbrella potential of 25 kcal·mol⁻¹·rad⁻² was moved along χ_1 at 10-deg intervals from 10° to 130°, and a 15-ps simulation was conducted following 5 ps of equilibration within each umbrella. The simulated system was solvated and constrained within a stochastic boundary as described above. Initially, an umbrella was applied at χ_1 = 70° to a dataset from the aforementioned solvated simulation and used as the "seed" structure. The last dataset from an adjacent umbrella was used to "prime" the simulation for each new umbrella.

As shown in Figure 4, the minimum barrier to χ_1 rotation appears to be at least 8 kcal/mol and occurs in the direction of positive χ_1 rotation. There is no observed tendency for rotation about χ_2 as χ_1 increases. A free energy minimum is found at ≈70° corresponding to the crystal structure value.

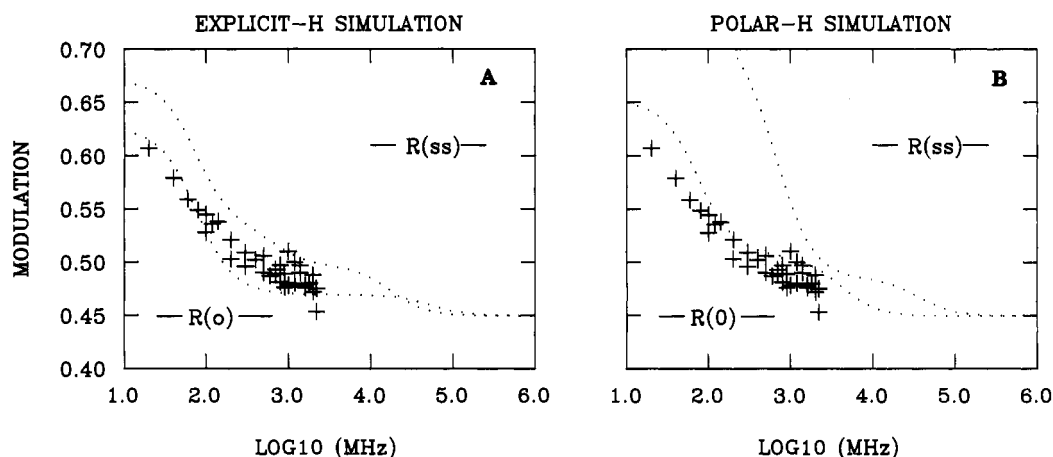EXPLICIT–H SIMULATION

POLAR–H SIMULATION

FIGURE 3: Comparison of experimental data and simulation results. Experimental modulation measurements [(+) same data in both graphs] are shown with the envelope predicted by the simulations (···). The envelope curves were derived according to the method given in the appendix from biexponential functions fit to the upper and lower curves shown in Figure 2, with terms added for the average fluorescence lifetime and the rotational correlation time of the protein [3.2 and 5.0 ns, respectively; taken from Eftink (1983)]. Modulation ratios corresponding to the anisotropy in the absence of motion (r_0) and the steady-state anisotropy (r_{ss}) are indicated. All realistic measurements and predictions should lie between these two values. The decay function envelopes of Figure 2 actually determine the graphs in this figure only for frequencies of >1000 MHz (i.e., >3.0 $\log_{10}$ MHz); however, they have been extrapolated to lower frequencies for illustration.
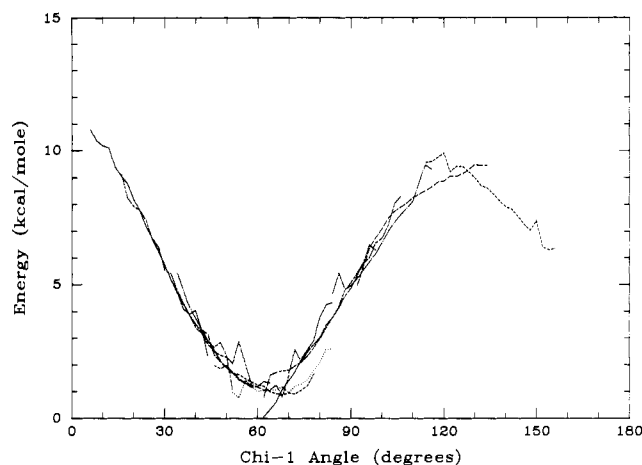
FIGURE 4: Helmholtz free energy for the rotation of Trp-3 about χ_1 by the method of Haydock et al. (1990). Umbrella potentials were moved at 10-deg increments in positive and negative directions from the crystal structure value ($\approx 70°$). The free energy for each umbrella is shown as a separate curve and in a distinct line style.

However, the crystal structure was used as a seed structure, so the significance of this correspondence remains to be shown by a more complete study including forward and backward rotation over 360°. We cite these results merely as theoretical evidence for a significant free energy barrier to Trp side-chain rotation. A more complete study would be needed to estimate barrier crossing rates and explore other (and possibly lower) free energy minima on the χ_1–χ_2 surface.

A comparison of the topology and parameter files used for the explicit-H and polar-H simulations suggested that the basis for their markedly different predictions might be related to the treatment of electrostatic charge in the Trp side chain. In order to preserve overall electroneutrality in the indole side chain, most atoms in the six-atom (benzyl) ring must be assigned a charge of 0.0 in polar-H models. In contrast, the C–H pairs in the explicit-H model are each given a slight dipolar character by assigned charges of $-0.1/+0.1$. This yields a side-chain model with electronegative ring faces and electropositive ring edges, mimicking an aromatic π-electron system.

To confirm the role of this charge distribution in influencing the rotational behavior of the Trp side chain, two further explicit-H simulations were conducted. In one, charges on the four C–H atom pairs in the six-atom ring of Trp were set to zero. In another, charges on all aromatic C–H atom pairs were set to zero. Neutralizing the charges only on the Trp side chain clearly increased the rotational activity of the side chain; however, the degree of rotational activity seen in the polar-H simulation was approximated only when all aromatic ring charges in the protein were neutralized (data not shown).

A specific consequence of altering the charge distributions in this way may be illustrated by looking at the interaction of the Trp side chain with water. When the Trp side chain is modeled with electronegative ring faces, there is a tendency for water hydrogens to form hydrogen bonds with the ring faces (Figure 5). When the side-chain dipoles are neutralized, these hydrogen bonds do not form. There is some directional preference seen for water seen at >3.5 Å from the Trp rings in both simulations, a consequence of water interacting with a nearby peptide N–H group.

Weakened interactions between water and aromatic side chains may not be the sole reason for the excessive rotational activity in the polar-H simulation. As shown in Figure 2, the excessive polar-H rotations are manifest at short times (≈ 100 ps), whereas excessive rotations in explicit-H simulations without aromatic dipoles are manifest only at longer times
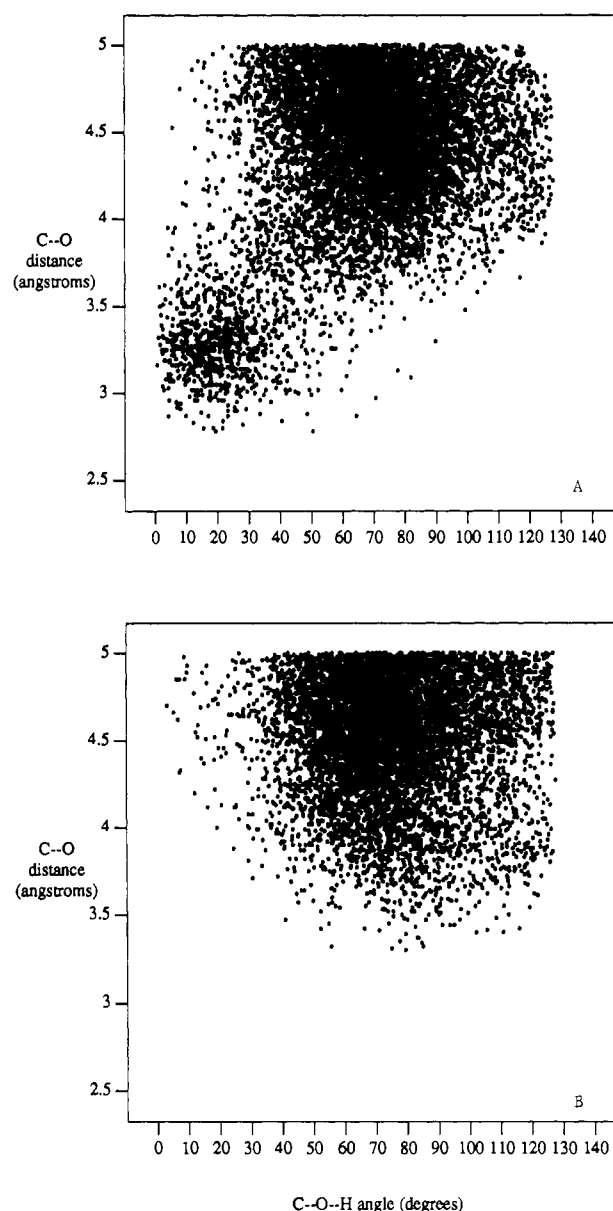

C–O–H angle (degrees)

FIGURE 5: Water orientations in the vicinity of Trp-3. The distance between a water oxygen and the center of the six-atom ring of Trp-3 is plotted against the orientation of the water with respect to the ring. The angle given is that formed by the nearest carbon atom in the Trp ring, the water oxygen, and the water hydrogen which is closest to the ring. Each point represents an occurrence in a 40-ps trajectory sampled every 0.02 ps. Only those waters below the plane of the six-atom ring (i.e., between the ring and the remainder of the protein) were included. In (A), the graph for the explicit-H simulation is shown, indicating numerous occurrences of an O–H bond oriented between 0° and 30° to an aromatic carbon and separated by less than 3.5 Å. In (B), the graph for the polar-H simulation is shown, indicating that few such relationships occur. Graphs for the explicit-H simulation without Trp ring dipoles and without any aromatic dipoles are indistinguishable from the polar-H graph.

(≈ 200–300 ps; data not shown). Thus, the presence or absence of aliphatic C–H dipoles may also be of consequence and requires further study.

DISCUSSION

These results suggest that use of the polar-H topology for simulating the rotational activity of the Trp side chain on the surface of PLA2 results in a serious predictive error. Although the explicit-H simulation is consistent with the experimental data, we must temper our confidence in the simulation by considering some of the limitations inherent in both the ex-

perimental and simulation techniques.

One of the experimental limitations results from the small magnitude of relatively short-lifetime components in PLA2. Specifically, Alcala et al. (1989) report exponential components of 5.39, 2.16, and 0.60 ns, with fractional contributions of 0.42, 0.43, and 0.15, respectively. As a consequence, signal modulation (m) approaches zero within the experimentally accessible frequency range because $m = (1 + \omega^2\tau^2)^{-1/2}$, where ω is the frequency in radians/second and τ is the lifetime of the excited state. For PLA2, a low signal-to-noise ratio precluded measurements beyond 3000 MHz, despite instrumental electronics intrinsically capable of measurements up to 10 GHz.

On the other hand, it is clear that very little rotational activity is unaccounted for at 3000 MHz. Using $r_0 = 0.29$, we determine the corresponding modulation ratio in the absence of motion (Λ_0) to be 0.45 (see Appendix). At 3000 MHz, we find $\Lambda = 0.48$ indicating that the anisotropy decays only from 0.290 to 0.265 during times which are too fast to measure. This corresponds to a rotational cone angle of 14° and compares reasonably well to the value of 17° derived by Eftink (1983) from limiting anisotropy determinations of the "apparent r_0" in PLA2 excited at 300 nm. In contrast to a limiting anisotropy, which is determined by means of a long extrapolation and the use of extrinsic quenchers, the device used in this work provides a direct measure of anisotropy decay at specific time intervals.

It is almost always appropriate to question whether the size and duration of a simulation is adequate. In this case, we consider less than half of the protein residues and water molecules only if they are within 16 Å of Trp-3. Furthermore, a 1-ns simulation is certainly not ergodic with respect to 1-ns events. The question of whether a simulation has been adequately "equilibrated" prior to data collection is perennial, and the answer clearly depends on the nature of the phenomenon under examination. We interpret the nonmonotonic decay functions of Figure 2 to indicate that either equilibration or low-frequency sampling is incomplete. Larger and longer simulations would certainly be desirable, but the calculations reported herein already required ≈40 CPU weeks on a 20-mips processor (equivalent to 48 CPU days using vector-optimized code on a CRAY-2). Having applied these resources, we can only claim that the explicit-H simulation appears far better than the polar-H simulation with respect to equilibration or completeness of sampling and that this advantage far outweighs the computational speed advantage accrued with the polar-H simulation.

Fortunately, the experimental data support the explicit-H simulation which predicts a lower modulation ratio (i.e., a higher anisotropy) than the polar-H simulation. This conveniently mitigates a number of concerns. For example, it is clear that constraints placed on the protein in the buffer zone adjacent to the boundary do not unrealistically constrain the protein—indeed, the problem with the polar-H simulation is excessive motion rather than too little. Likewise, we reason that the water models are not excessively packed within the boundary; if they were, they could limit rotational excursions of the side chain. We recognize that the size of the system limits our sampling of statistically probable local potential energy fluctuations (Cooper, 1984); but again, we must explain the excessive fluctuations found in the polar-H simulation rather than fluctuations which are too small.

The same number of (TIP3P) water molecules and the same initial water positions were used for both simulations. Therefore, any enhancing effect of solvent on surface-residue

fluctuations should be present in both simulations (Brooks & Karplus, 1989). Of note, both simulations predicted negligible Trp side-chain motions in preliminary simulations conducted in vacuo (data not shown). We suspect that the latter simulations have little value, however, because other portions of the protein structure deviated markedly and progressively from the original protein crystal structure; this behavior resembled unrealistic behaviors noted previously in simulations of ribonuclease T_1 conducted in vacuo (Axelsen et al., 1988).

It is more difficult to address problems related to the classical treatment of quantum-mechanical phenomena, particularly when we use only a single model for Trp which supposedly mimics a ground-state residue. We do not know whether the protein environment can alter the relative orientation of the absorption and emission dipoles of Trp or whether the electrostatic character of the excited state alters the rotational activity of the side chain. However, Weaver et al. (1988) have found good correlations between order parameters and rotational rates determined by the use of ^{13}C NMR relaxation measurements and fluorescence spectroscopy. The NMR method provides an independent measure of Trp side-chain dynamics and supports the interpretation of the fluorescence anisotropy measurements used in this work.

PLA2 exhibits a markedly nonexponential fluorescence intensity decay; at least three components or a distributed model must be invoked to adequately fit the data to an exponential model (Alcala et al., 1987). If this corresponds to three distinct conformations or physicochemical environments for Trp in PLA2, we cannot presume to have adequately sampled these environments in the simulation. However, the use of $\tau = 600$ or 5390 ps (the shortest and longest components reported by Alcala) for generating the curves in Figure 3 causes virtually no change in the curve at >1000 MHz, and thus, these alternative choices for τ cannot reconcile the polar-H simulation with the experimental data. Moreover, modulation ratios reach plateau or "steady-state" values when the simulation data are extrapolated to extreme low frequencies (left end of dotted curves in Figure 3), and these values may be converted to steady-state anisotropy. We find that using $\tau = 3200$ ps [Eftink, 1983; the τ_{ave} for values reported by Alcala et al. (1987)] for such extrapolations compares far better to our measurements of steady-state anisotropy than either $\tau = 600$ ps or $\tau = 5390$ ps (data not shown).

The difference between polar-H and explicit-H simulations appears to be due to differences in their treatment of aromatic ring electrostatics. An explicit-H simulation will reproduce much of the excessive rotational activity seen in the polar-H simulation if the C–H dipoles on aromatic rings are neutralized. At least one consequence of this modification is that the six-atom ring of Trp-3 can no longer be a hydrogen-bond acceptor for water. We often see a single water molecule simultaneously hydrogen bonding to the Trp ring face and the hydroxyl group of Tyr-75, with an interaction energy between the water and the Trp-3 side chain exceeding 5 kcal/mol. By its appearance, this structure suggests that the water molecule is tethering the Trp side chain to the protein surface and that this is the basis for hindered rotations of Trp-3.

An increasing body of evidence indicates that the ability of aromatic rings to serve as hydrogen-bond acceptors is real and significant to the structure and function of proteins (Burley & Petsko, 1985; Levitt & Perutz, 1988). Our work suggests that highly inaccurate simulations may result if the capacity to form such bonds is not incorporated into aromatic models. It seems doubtful that the polar-H model can be suitably modified while retaining the same number of atom centers.

However, explicitly including aromatic ring hydrogens in an otherwise polar-H simulation would add only 82 atoms and retain much of the computational advantage of the polar-H approach. In some cases, this approach has already been applied to proteins (Robson & Platt, 1986).

The molecular mechanics approach is fraught with severe approximations, most of which are made knowingly for the sake of computational feasibility. These circumstances underscore the need for experimental data which test and refine the approach. But, molecular mechanics is virtually our only means of exploring the structural basis of fine dynamic phenomena in proteins. It is especially important when the protein crystal structure cannot answer the question being asked. The simulations we report herein suggest an explanation for the limited rotational activity of Trp-3 that was not predicted from the crystal structure. Furthermore, they support a molecular-mechanical interpretation of anisotropy decay and enhance the value of anisotropy measurements for the exploration of protein structure and function.

APPENDIX

We seek the frequency-dependent modulation ratio, $\Lambda(\omega)$, in terms of the time-dependent anisotropy decay function, $r(t)$, which may be derived from a molecular dynamics simulation. We obtain the needed expression by first expressing the time-dependent intensity functions in terms of time-dependent anisotropy:

$$I_\perp(t) = [1 - r(t)]e^{-t/\tau}$$

$$I_\parallel(t) = [1 + 2r(t)]e^{-t/\tau}$$

where τ is the lifetime of the fluorophore and $I_\perp$ and $I_\parallel$ are the polarized fluorescence intensities perpendicular and parallel to the polarized excitation source. The modulation ratio is related to these signal intensities by $\Lambda = I_\perp/I_\parallel$. Since these expressions are valid in both time and frequency domains, $\Lambda(\omega)$ may be related to the Fourier transform of $I_\perp(t)/I_\parallel(t)$. These expressions also show that modulation ratios and anisotropies are related by $\Lambda = (1 - r)/(1 + 2r)$ in either the time or frequency domain.

Given that the time-dependent anisotropy of a fluorophore decays according to the sum of exponential terms

$$r(t) = r_0\sum_i g_i e^{-t/\phi_i}$$

where r_0 is the anisotropy in the absence of motion, g is a weighting factor, and ϕ is the rotational correlation time, and given that segmental motions may be represented by the product of exponentials

$$r(t) = r_0[\alpha e^{-t/\phi_F} + (1 - \alpha)]e^{-t/\phi_P}$$

where α is a weighting factor and subscripts F and P refer to fluorophore and protein, respectively, it follows that a double-exponential decay attributable to segmental motion may be represented by

$$r(t) = r_0[\alpha\beta e^{-t/\phi_{F'}} + \alpha(1 - \beta)e^{-t/\phi_{F''}} + (1 - \alpha)]e^{-t/\phi_P}$$

where α is the fraction of decay due to segmental motions and β is the fraction of decay attributable to the first of the two exponential decay components. We may insert this expression into expressions given above for $I_\perp$ and $I_\parallel$. The resulting expressions are

$$I_\perp(t) = e^{-tk} - r_0[\alpha\beta e^{-tk'} + \alpha(1 - \beta)e^{-tk''} + (1 - \alpha)e^{-tk'''}]$$

$$I_\parallel(t) = e^{-tk} + 2r_0[\alpha\beta e^{-tk'} + \alpha(1 - \beta)e^{-tk''} + (1 - \alpha)e^{-tk'''}]$$

where

$$k = \tau \qquad k' = \left(\frac{1}{\phi_{F'}} + \frac{1}{\phi_P} + \frac{1}{\tau}\right)^{-1}$$

$$k'' = \left(\frac{1}{\phi_{F''}} + \frac{1}{\phi_P} + \frac{1}{\tau}\right)^{-1} \qquad k''' = \left(\frac{1}{\phi_P} + \frac{1}{\tau}\right)^{-1}$$

These expressions may, in turn, be analytically transformed into the frequency domain, whereupon

$$\text{Re}[I_\perp(\omega)] = \frac{k}{1 + (\omega k)^2} - r_0\left[\frac{\alpha\beta k'}{1 + (\omega k')^2} + \frac{\alpha(1 - \beta)k''}{1 + (\omega k'')^2} + \frac{(1 - \alpha)k'''}{1 + (\omega k''')^2} + \right]$$

$$\text{Re}[I_\parallel(\omega)] = \frac{k}{1 + (\omega k)^2} + 2r_0\left[\frac{\alpha\beta k'}{1 + (\omega k')^2} + \frac{\alpha(1 - \beta)k''}{1 + (\omega k'')^2} + \frac{(1 - \alpha)k'''}{1 + (\omega k''')^2} + \right]$$

$$\text{Im}[I_\perp(\omega)] = \frac{k^2\omega}{1 + (\omega k)^2} - r_0\left[\frac{\alpha\beta k'^2\omega}{1 + (\omega k')^2} + \frac{\alpha(1 - \beta)k''^2\omega}{1 + (\omega k'')^2} + \frac{(1 - \alpha)k'''^2\omega}{1 + (\omega k''')^2} + \right]$$

$$\text{Im}[I_\parallel(\omega)] = \frac{k^2\omega}{1 + (\omega k)^2} + 2r_0\left[\frac{\alpha\beta k'^2\omega}{1 + (\omega k')^2} + \frac{\alpha(1 - \beta)k''^2\omega}{1 + (\omega k'')^2} + \frac{(1 - \alpha)k'''^2\omega}{1 + (\omega k''')^2} + \right]$$

allowing $\Lambda(\omega)$ to be calculated from the frequency-dependent intensity amplitudes given by

$$I_\perp = \sqrt{\text{Re}^2(I_\perp) + \text{Im}^2(I_\perp)}$$

$$I_\parallel = \sqrt{\text{Re}^2(I_\parallel) + \text{Im}^2(I_\parallel)}$$

REFERENCES

Alcala, J. R., Gratton, E., & Prendergast, F. G. (1987) *Biophys. J. 51*, 925–936.

Allegrini, P. R., van Scharrenburg, G. J. M., Slotboom, A.. J., de Haas, G. H., & Selig, J. (1985) *Biochemistry 24*, 3268–3273.

Axelsen, P. H., & Prendergast, F. G. (1989) *Biophys. J. 56*, 43–66.

Axelsen, P. H., Haydock, C., & Prendergast, F. G. (1988) *Biophys. J. 54*, 249–258.

Bash, P. A., Singh, U. C., Brown, F. K., Langridge, R., & Kollman, P. A. (1987) *Science 235*, 574–576.

Bernstein, F. C., Keotzle, T. F., Williams, G. J. B., Meyer, E. F., Brice, M. D., Rodgers, J. R., Kennard, O., Shimanouchi, T., & Tasumi, M. (1977) *J. Mol. Biol. 112*, 535–542.

Brooks, B. R., Bruccoleri, R. E., Olafson, B. D., States, D. J., Swaminathan, S., & Karplus, M. (1983) *J. Comp. Chem.* *4*, 187–217.

Brooks, C. L., III, & Karplus, M. (1989) *J. Mol. Biol. 208*, 159–181.

Brooks, C. L., III, Brunger, A., & Karplus, M. (1985) *Biopolymers 24*, 843–865.

Burley, S. K., & Petsko, G. A. (1985) *Science 229*, 23–28.

Burley, S. K., & Petsko, G. A. (1986) *FEBS Lett. 203*, 139–143.

Cooper, A. (1984) *Prog. Biophys. Mol. Biol. 44*, 181–214.

Dijkstra, B. W., Renetseder, R., Kalk, K. H., Hol, W. G. J., & Drenth, J. (1983) *J. Mol. Biol. 168*, 163–168.

Eftink, M. (1983) *Biophys. J. 43*, 323–334.

Ghosh, I., & McCammon, J. A. (1987) *Biophys. J. 51*, 637–641.

Haydock, C., Sharp, J., & Prendergast, F. G. (1990) *Biophys. J. 57*, 1269–1279.

Ichiye, T., & Karplus, M. (1983) *Biochemistry 22*, 2884–2893.

Lakowicz, J. R., Laczko, G., Gryczynski, I., & Cherek, H. (1986) *J. Biol. Chem. 261*, 2240–2245.

Lakowicz, J. R., Laczko, G., & Gryczynski, I. (1987) *Biochemistry 26*, 82–90.

Levitt, M., & Perutz, M. F. (1988) *J. Mol. Biol. 201*, 751–754.

Robson, B., & Platt, E. (1986) *J. Mol. Biol. 188*, 259–281.

Valeur, B., & Weber, G. (1977) *Photochem. Photobiol. 25*, 441–444.

Weaver, A. J., Kemple, M. D., & Prendergast, F. G. (1988) *Biophys. J. 54*, 1–15.

Weber, G. (1977) *J. Chem. Phys. 66*, 4081–4091.

Yamamoto, Y., & Tanaka, J. (1970) *Biochim. Biophys. Acta 207*, 522–531.

Articles

Conformation of Thiocolchicine and Two B-Ring-Modified Analogues Bound to Tubulin Studied with Optical Spectroscopy

Per Lincoln,[‡] Jerker Nordh,[‡] Johanna Deinum,[§] Jonas Ångström,[∥] and Bengt Nordén*[‡]

Department of Physical Chemistry, Chalmers University of Technology, S-412 96 Gothenburg, Sweden, and Departments of Medical Physics and Medical Biochemistry, University of Gothenburg, S-400 33 Gothenburg, Sweden

ABSTRACT: The interaction of tubulin with thiocolchicine and two thiocolchicine analogues, one lacking the B ring and one with a six-membered B ring, has been studied by using near-UV and CD spectroscopies. Rapid, reversible binding of the latter analogue to tubulin demonstrates the ability of the colchicine binding site to accommodate the phenyltropone system with a more coplanar conformation than is present in free colchicine. There is no evidence, however, that bound thiocolchicine should have a much less twisted conformation than free thiocolchicine. Thiocolchicine and the bicyclic analogue appear to have approximately the same conformation of the phenyltropone system, in both the free and the bound states, suggesting that this conformation has an optimal arrangement of the phenyl and tropone rings for binding to tubulin. In contrast to colchicine and related derivatives, the three thiocolchicine analogues show pronounced near-UV CD bands upon association to tubulin. No simple relation could be found between the sign pattern of the CD components in the near-UV band of the thiocolchicinoid chromophore and its axial chirality.

Colchicine (Chart I), the classical mitosis-inhibiting alkaloid from *Colchicum autumnale*, mainly exerts its physiological activity by forming a stable 1:1 complex with the tubulin protein, thereby interfering with its assembly to microtubuli (Bryan, 1972; Olmsted & Borisy, 1973; Sternlicht & Ringel, 1979; Farell & Wilson, 1984). Colchicine is not covalently bound to tubulin, but the high activation energy for binding and dissociation makes the binding slow and practically irreversible (Garland, 1978; Lambeir & Engelborghs, 1981). Studies of more simple analogues of colchicine have shown that the trimethoxybenzene and methoxytropone rings each bind to distinct sites (Cortese et al., 1977; Andreu & Timasheff, 1982a,b) and that the direct linkage of the rings, by virtue of a chelate effect, is a prerequisite for high binding affinity (Andreu et al., 1984). The B ring, including its

Chart I

Thiocolchicine (1)   X = CH₃S
Colchicine   X = CH₃O
(2)   X = CH₃S
MTC   X = CH₃O
(3)
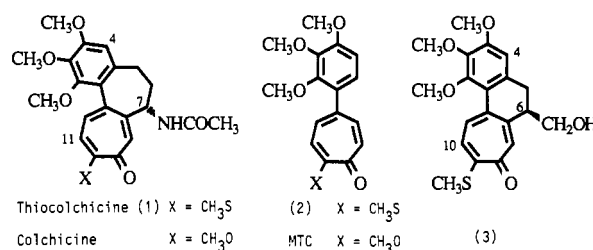
substituents, has a major influence on the association/dissociation kinetics (Bhattacharyya et al., 1986; Banerjee et al., 1987). For example, the bicyclic colchicine analogue MTC[1]

[‡] Chalmers University of Technology.
[§] Department of Medical Physics, University of Gothenburg.
[∥] Department of Medical Biochemistry, University of Gothenburg.

[1] Abbreviations: CD, circular dichroism; DMSO, dimethylsulfoxide; LD, linear dichroism; LDʳ, reduced linear dichroism; MCD, magnetic circular dichroism; MTC, 2-methoxy-5-(2′,3′,4′-trimethoxyphenyl)-2,4,6-cycloheptatrien-1-one; Pipes, 1,4-piperazinediethanesulfonic acid; PVA, poly(vinyl alcohol).